Heavily Tungsten Doped Sodium Thioantimonate Solid State Electrolytes (SSEs) with Exceptionally Low Activation Energy for Ionic Diffusion

Xuyong Feng[1#], Hong Fang[2#], Pengcheng Liu[1], Nan Wu[1], Ethan Self [3], Liang Yin[4], Pengbo Wang[5], Xiang Li[6], Puru Jena[2], Jagjit Nanda[3*], David Mitlin[1*]

[#] These authors contributed equally

[1] Materials Science and Engineering Program & Texas Materials Institute (TMI), The University of Texas at Austin, Austin, TX 78712-1591, USA

[2] Department of Physics, Virginia Commonwealth University, Richmond, VA 23284, USA

[3] Chemical Sciences Division, Oak Ridge National Laboratory, Oak Ridge, TN 37830, USA

[4] X-ray Science Division, Argonne National Laboratory, 9700 South Cass Avenue, Lemont, IL 60439, USA

[5] Department of Chemistry and Biochemistry, Florida State University, Tallahassee, FL 32306, USA

[6] Argonne National Laboratory, 9700S. Cass Avenue, Lemont, IL 60439, USA

* nandaj@ornl.gov, *david.mitlin@austin.utexas.edu

Abstract

Using multiple synergistic design rules, we put forward a powerful strategy to reduce the activation energy for cation diffusion by modifying the structure of solid-state electrolytes (SSEs). Two heavily W-doped sodium thioantimonate SSEs, $Na_{2.895}W_{0.3}Sb_{0.7}S_4$ and $Na_{2.7}W_{0.3}Sb_{0.7}S_4$ are designed, both exhibiting exceptionally low activation energy for sodium ion diffusion and enhanced room temperature (RT) ionic conductivity; 0.09 eV, 24.2 mS/cm and 0.12 eV, 14.5 mS/cm. The 30% W content goes far beyond the 10-12% reported in the prior studies, and results in novel pseudo-cubic or orthorhombic structures. Theoretical studies based on density functional theory (DFT) calculations reveal that these properties result from a combination of multiple diffusion mechanisms, including vacancy defects, strongly correlated modes and excessive Na-ions. An all-solid-state battery (ASSB) using $Na_{2.895}W_{0.3}Sb_{0.7}S_4$ as the primary SSE and a sodium sulfide (Na_2S) cathode achieves a reversible capacity of 400 mAh/g.

Keywords: Na_3SbS_4, superionic conductor, sodium - sulfur battery, Solid-State Battery (SSB), sodium metal battery (SMB).

Introduction

Employing solid-state electrolytes (SSEs) rather than liquid organic electrolytes is a possible path towards greater battery safety since most inorganic SSE's are non-flammable.[1–19] Recently, there has been significant progress related to a number of successful solid-state battery chemistries showing reasonable cycle-life and capacity retention using traditional cathodes of Li-ion battery (LIB) and metal anodes.[20,21] The success of this technology hinges on developing practical superionic conducting SSEs with robust electrochemical stability.[22–24] The future of solid-state batteries is not limited to Li-metal batteries only.[25–34] Progress in Na and K metal anodes and related solid-state ionic conductors[35–37] provide a potential path for safe sodium metal batteries and possibly potassium metal batteries. SSE and all solid state batteries (ASSBs) based sodium thioantimonate (Na_3SbS_4) and related Na_3PnS_4 (Pn = P, As, Sb) are attracting interest due to their ambient temperature ionic conductivity.[36–66] The undoped Na_3SbS_4 has been reported to achieve 0.6 mS/cm in its room temperature (RT) tetragonal phase [68], with markedly increased conductivity occurring in the elevated temperature phases. [53,69] Authors reported that light W-doping at the Sb sites ($Na_{2.88}W_{0.12}Sb_{0.88}S_4$ and $Na_{2.9}W_{0.1}Sb_{0.9}S_4$) can stabilize the high temperature cubic structure at ambient temperature, boosting the RT ionic conductivity to 41($\pm$ 8) mS/cm.[6-7]

The high RT ionic conductivity achieved in these systems has been attributed to the introduction of Na-vacancies caused by W^{6+} substituting Sb^{5+}. A small number of Na-vacancies can generate a large number of degenerate or near-degenerate energy states, which allow the Na-ions to diffuse and rearrange. For example, two Na-vacancies out of 48 Na sites in a $2 \times 2 \times 2$ Na_3SbS_4 supercell corresponds to a concentration similar to the cases of $Na_{2.88}W_{0.12}Sb_{0.88}S_4$ and $Na_{2.9}W_{0.1}Sb_{0.9}S_4$. The result is $C_{48}^{46} = C_{48}^{2} = 1128$ possible configurations for the Na sublattice. This is in contrast with the single ground state of the Na sublattice in a defect-free tetragonal or cubic Na_3SbS_4, where the ionic diffusion relies solely on the collective motion of Na-ions in rows without individual jumps through vacancies.[70,71] Although the presence of Na-vacancies may provide a significant "add-on" to the enhancement of ionic conductivity, its implication on the activation energy is not straightforward. This is evidenced by the measured activation energies, 0.21 and 0.18 eV, of the cubic $Na_{2.88}W_{0.12}Sb_{0.88}S_4$ and $Na_{2.9}W_{0.1}Sb_{0.9}S_4$, respectively, [6-7] which are much larger than that ($\leq$ 0.08 eV) of the cubic phase of Na_3SbS_4.[64,69] The activation energy,

corresponding to the energy barrier of individual diffusion steps, should be largely determined by the local Na-Na and Na-S interactions in the system. The high activation energy of $Na_{2.88}W_{0.12}Sb_{0.88}S_4$ and $Na_{2.9}W_{0.1}Sb_{0.9}S_4$ may be due to the tetragonal local structure, like cubic glass-ceramic Na_3PS_4 sintered at 260 ℃.[49] Therefore, fine tuning the local environment of the Na-ion is the key for the reduction of the activation energy.

Here, we tune the structure and the resultant ionic conductivity/activation energy of W-doped Na_3SbS_4 by greatly extending the W content, going far beyond the 10-12% reported in the previous studies. [6-7] A heavily W-doped system $Na_{2.7}W_{0.3}Sb_{0.7}S_4$, is successfully synthesized, and is demonstrated to display an orthorhombic structure. This new phase displays a high RT ionic conductivity of 14.5 mS/cm and a uniquely low activation energy of 0.12 eV. The properties are further optimized by tuning the Na-ion/vacancy content of the material, resulting in $Na_{2.895}W_{0.3}Sb_{0.7}S_4$ with an enhanced RT ionic conductivity of 24.2 mS/cm and a record low activation energy of 0.09 eV.

Results and Discussion

W-doped Na-Sb-W-S systems, $Na_{3-x}W_xSb_{1-x}S_4$ (x = 0.1, 0.2 and 0.3), are prepared using the method described in the Supporting Information (SI). To obtain a reliable structural model for the heavily W-doped $Na_{2.7}W_{0.3}Sb_{0.7}S_4$, we generated all possible configurations with the given chemical formula based on a 2×2×2 supercell of Na_3SbS_4 in which five Sb sites are substituted by W atoms and five Na-vacancies are created at the same time. Given the total of 16 Sb and 48 Na sites in the supercell, there are C_{16}^5 and C_{48}^5 number of possible combinations, respectively, for the substitution and the vacancy creation. Therefore, a total of $C_{16}^5 \times C_{48}^5 = 7.5\times10^9$ configurations were considered. Their total electrostatic energies based on point-charge models are computed using the Ewald summation and are ranked accordingly. The configurations having the lowest energies are further subjected to density functional theory (DFT) optimizations and calculations. The ground-state structure of $Na_{2.7}W_{0.3}Sb_{0.7}S_4$ identified from the procedure is shown in **Figure 1A**. It is found that all the five W atoms occupy the high-symmetry sites in the cell, including one at the body center, one at the face center and three at the edge centers. The five Na-vacancies are situated at the neighboring sites of the doped W atoms.

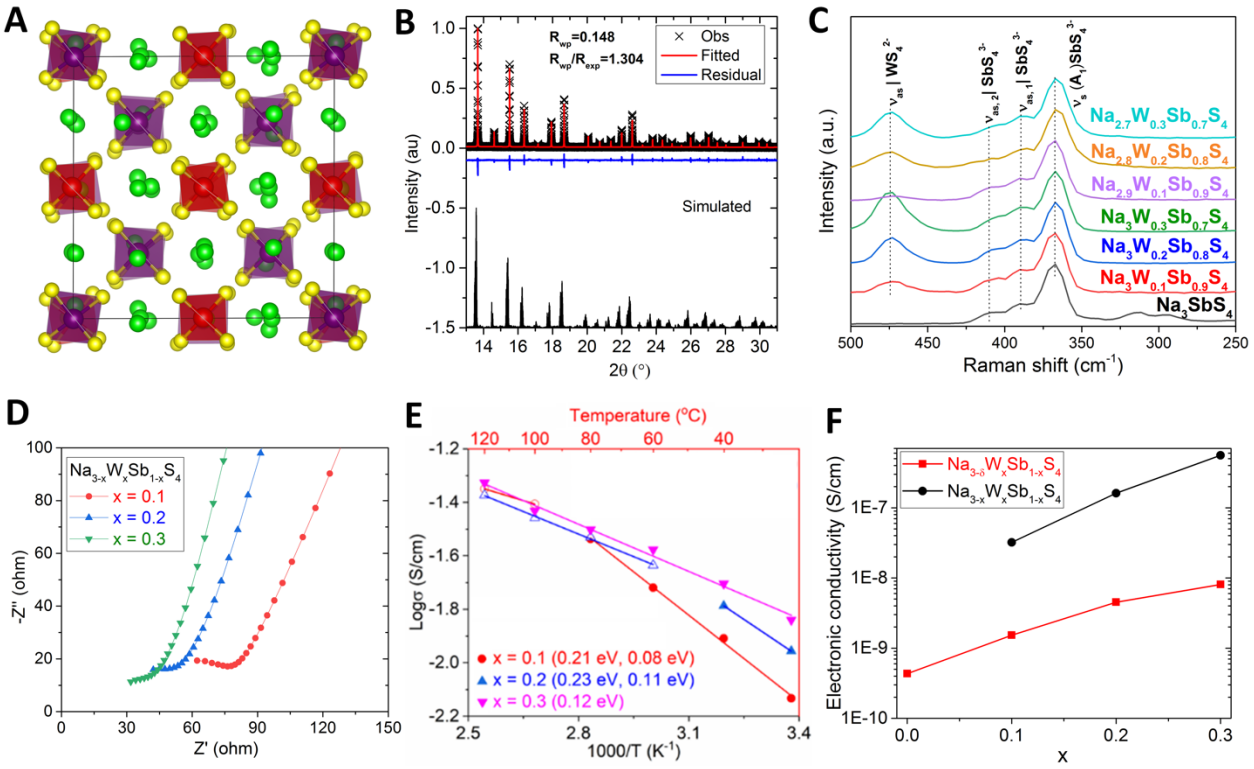

Fig. 1 Characterization $Na_{2.7}W_{0.3}Sb_{0.7}S_4$. (**A**) Theoretically identified ground-state structure of $Na_{2.7}W_{0.3}Sb_{0.7}S_4$ with SbS_4^{3-} units in purple, WS_4^{2-} units in red and Na in green. (**B**) Synchrotron XRD of $Na_{2.7}W_{0.3}Sb_{0.7}S_4$ and the Rietveld refinement based on an orthorhombic structure. (**C**) The Raman spectra of the synthesized $Na_{3-x}W_xSb_{1-x}S_4$ and $Na_{3-\delta}W_xSb_{1-x}S_4$ (x = 0.1, 0.2 and 0.3; $0 < \delta < x$) series compared to that of tetragonal Na_3SbS_4. (**D**) The measured AC impedances for the $Na_{3-x}W_xSb_{1-x}S_4$ (x = 0.1, 0.2 and 0.3) series. (**E**) The measured ionic conductivities of the $Na_{3-x}W_xSb_{1-x}S_4$ (x = 0.1, 0.2 and 0.3) series at different temperatures. (**F**) Measured electric conductivities of the $Na_{3-x}W_xSb_{1-x}S_4$ and $Na_{3-\delta}W_xSb_{1-x}S_4$ (x = 0.1, 0.2 and 0.3; $0 < \delta < x$) series.

As shown in **Figure 1B**, the Rietveld refinement (see SI) based on the structural model shows that $Na_{2.7}W_{0.3}Sb_{0.7}S_4$ has an orthorhombic structure with lattice parameters a=14.3762, b=14.3757 and c=14.3774 Å. The DFT optimized lattice parameters (a=14.5332, b=14.4798 and c=14.5407) are in good agreement with the experimental ones with relative differences $\leq$ 1%. No obvious phase fraction is observed in the XRD of $Na_{2.7}W_{0.3}Sb_{0.7}S_4$, as compared to the XRDs of the pristine Na_3SbS_4 and $Na_{3-x}W_xSb_{1-x}S_4$ (x = 0.1 and 0.2) in the series (**Figure S1** of SI). The Raman spectrum of $Na_{2.7}W_{0.3}Sb_{0.7}S_4$ is also compared to those of the pristine Na_3SbS_4 and $Na_{3-x}W_xSb_{1-x}S_4$ (x = 0.1

and 0.2) and no peaks belonging to impurities (e.g., crystal WS_2) are found, as shown in **Figure 1C**. The three Raman signals around 370, 390, and 410 cm^{-1} correspond to the different modes of SbS_4^{3-} tetrahedra, and the peak around 470 cm^{-1} signals the presence of WS_4^{2-} units in the doped system.

AC impedances are measured for the studied Na-Sb-W-S systems, as shown in **Figure 1D**. With increasing W-doping in the system, the bulk resistance decreases from 78 Ω in $Na_{2.9}W_{0.1}Sb_{0.9}S_4$ to 52 Ω in $Na_{2.8}W_{0.2}Sb_{0.8}S_4$, and then to 40 Ω in $Na_{2.7}W_{0.3}Sb_{0.7}S_4$. These correspond to the increasing ionic conductivities in **Figure 1E**, with $Na_{2.7}W_{0.3}Sb_{0.7}S_4$ exhibiting the highest RT ionic conductivity of 14.5 mS among the series. No sudden change in the ionic conductivity of $Na_{2.7}W_{0.3}Sb_{0.7}S_4$ that would break the linearity of the Arrhenius relation is observed, suggesting that there is no phase transition of the material. The measured activation energy of $Na_{2.7}W_{0.3}Sb_{0.7}S_4$ is 0.12 eV which is the lowest among the known Na-Sb-W-S systems so far (see **Table 1**). On the other hand, discontinuities do occur in the ionic conductivities of $Na_{2.9}W_{0.1}Sb_{0.9}S_4$ and $Na_{2.8}W_{0.2}Sb_{0.8}S_4$ at about 90 and 50 ℃, respectively, indicating phase transitions of these systems around the corresponding temperatures. The phase transitions greatly increase the activation energies of $Na_{2.9}W_{0.1}Sb_{0.9}S_4$ and $Na_{2.8}W_{0.2}Sb_{0.8}S_4$, from the high-temperature values of only 0.08 and 0.11 eV, respectively, to the RT values of 0.21 and 0.23 eV. The measured electron conductivities (**Figure S2** and **Figure 1F**) show that $Na_{2.7}W_{0.3}Sb_{0.7}S_4$ and the others in the series are all good insulators, supporting their applications as solid electrolytes.

A systematic theoretical study (Theoretical Methods in SI) is carried out to unravel the fast-ion conduction mechanism and the implications of the heavy W-doping in $Na_{2.7}W_{0.3}Sb_{0.7}S_4$. As shown in **Figure 2A**, there are three types of Na-vacancies in the obtained structural model. Type 1 sits between two doped W-ions, type 2 between one Sb and one W ion, and type 3 between two Na-ions. Due to their different local environments, the energy barriers for a neighboring Na-ion to migrate into these vacancies are also different, with type 1 having the highest energy barrier of 0.12 eV and the other two types having barriers less than 0.04 eV (40 meV). Diffusivities and ionic conductivities of $Na_{2.7}W_{0.3}Sb_{0.7}S_4$ are calculated based on molecular dynamics simulations at a few temperatures and extrapolated to other temperatures according to the Arrhenius relation, as shown in **Figure 2B**. The extracted activation energy of 0.101 eV is consistent with the value from

the static calculation in **Figure 2A** and in good agreement with the experimental value of 0.12 eV. The obtained theoretical ionic conductivity at RT is 145 mS/cm which is an order of magnitude higher than the measured value of 14.5 mS/cm. The calculated ionic conductivity is commonly known to be significantly higher than the experimental one,[72] since the measured value is limited by the preparation quality and the contained grain boundaries in the sample, which can reduce the ionic conductivity by up to 1-2 orders of magnitude.[73] Indeed, it is found that $Na_{2.7}W_{0.3}Sb_{0.7}S_4$ tends to form grain boundaries with large ionic resistance in the powder sample, as shown in **Figure S3**.

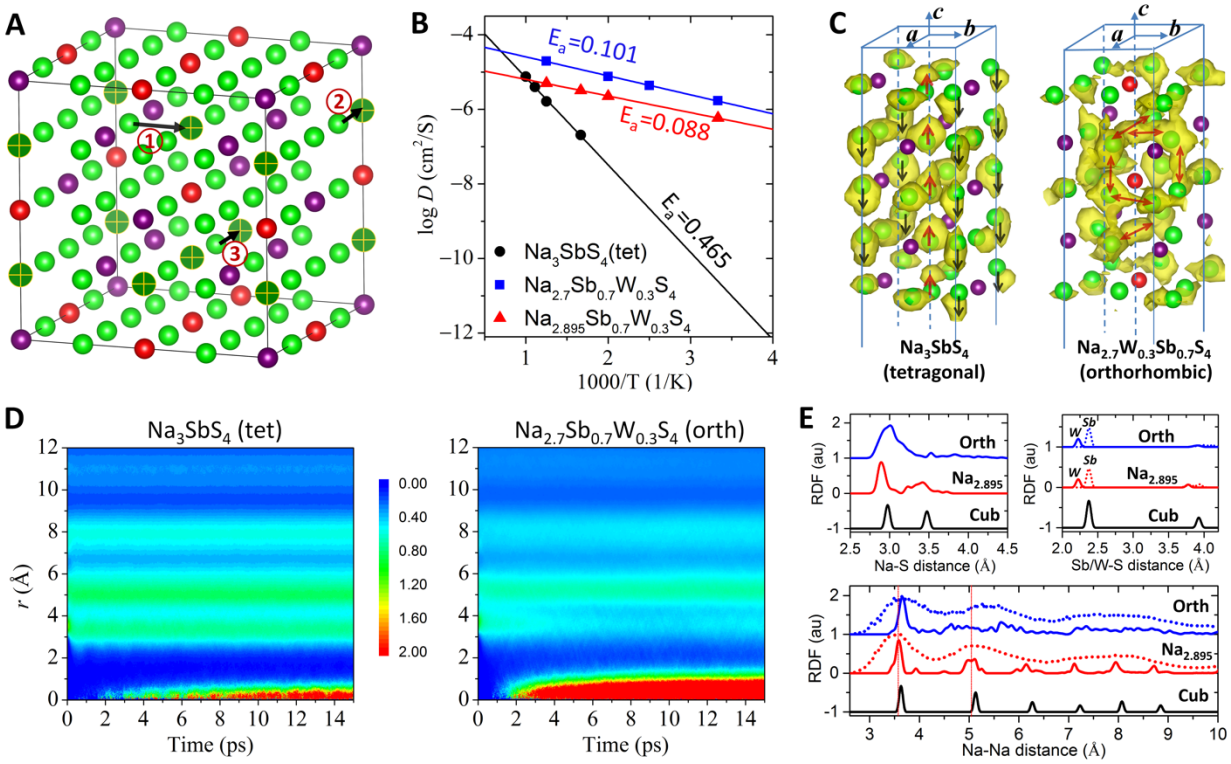

Fig. 2 Theoretical studies on the fast-ion transport in $Na_{2.7}W_{0.3}Sb_{0.7}S_4$ and $Na_{2.895}W_{0.3}Sb_{0.7}S_4$. (**A**) The theoretically obtained structure model for the ground state of the heavily W-doped $Na_{2.7}W_{0.3}Sb_{0.7}S_4$ based on a 2×2×2 supercell of Na_3SbS_4 (see Theoretical Method in SI). (**B**) Calculated diffusivities of $Na_{2.7}W_{0.3}Sb_{0.7}S_4$ and $Na_{2.895}W_{0.3}Sb_{0.7}S_4$ at different temperatures fitted by the Arrhenius relation, compared to the case of tetragonal Na_3SbS_4. (**C**) Calculated probability distribution functions for the defect-free tetragonal Na_3SbS_4 and $Na_{2.7}W_{0.3}Sb_{0.7}S_4$. Iso-surfaces (in yellow) with the same probability value are shown

for both materials. Na atoms are in light green, Sb in purple, and W in red. S atoms are not shown. Without any Na-vacancy, the tetragonal Na_3SbS_4 acts like a one-dimensional ionic conductor along the *c*-axis, featured by rows of Na-ions moving collectively. This is shown by the protruded probability surfaces around each Na-ion to the same direction along the axis. The neighboring Na rows are moving in the opposite directions, as indicated by the red and black arrows, to lower the electrostatic energy. On the other hand, three-dimensional ionic diffusion is found in $Na_{2.7}W_{0.3}Sb_{0.7}S_4$, featured by both individual jumps to vacancies as well as correlated motions in the rows of Na-ions. (**D**) Calculated van Hove correlation function of Na-ions in the defect-free tetragonal (tet) Na_3SbS_4 and orthorhombic (orth) $Na_{2.7}W_{0.3}Sb_{0.7}S_4$, showing strong Na-Na correlational modes around 3, 5 and 8 Å corresponding to the third nearest neighbors. (**E**) Calculated Na-S, Sb/W-S and Na-Na radial distribution functions (RDF) for the orthorhombic $Na_{2.7}W_{0.3}Sb_{0.7}S_4$ (Orth) and pseudo-cubic $Na_{2.895}W_{0.3}Sb_{0.7}S_4$ ($Na_{2.895}$), compared to those of the cubic phase of Na_3SbS_4 (Cub) which exhibits the exceptionally low activation energy. For $Na_{2.7}W_{0.3}Sb_{0.7}S_4$ and $Na_{2.895}W_{0.3}Sb_{0.7}S_4$, Na-Na, RDFs calculated from the structure snapshots obtained from molecular dynamics simulations over 100 ps are also given (in dotted profiles). The three peaks shown in the blue dotted curve correspond to the strong Na-Na correlational modes around 3, 5 and 8 Å in the van Hove correlation function of $Na_{2.7}W_{0.3}Sb_{0.7}S_4$.

The importance of W-doping on the Na-ion diffusion can be seen by comparing $Na_{2.7}W_{0.3}Sb_{0.7}S_4$ to the defect-free Na_3SbS_4. Without W dopant and Na-vacancy, Na-ion diffusion in tetragonal Na_3SbS_4 can only rely on the collective motion in a row and the material acts like a one-dimensional ionic conductor along the *c*-axis, as shown by the calculated probability distribution in **Figure 2C**. This originates from the structure feature of the Na-Sb-S system. There are two types of cationic rows arranged alternately along each crystalline axis of the structure. One type containing only Na-ions (•••Na-Na-Na-Na•••) can support the collective diffusion, while the other type containing alternate Na and immobile Sb ions (•••Na-Sb-Na-Sb•••) cannot. For the tetragonal phase of Na_3SbS_4, rows of Na-ions along the *a* and *b* axes are coordinated by alternate 6 and 8 S neighbors with short averaged Na-S bond length, which entails great energy cost (with an energy barrier of 0.65 eV[71]) for the Na-ions to diffuse along these axes. Along the *c* axis, on the other hand, Na-ions in a row are coordinated by 6 S neighbors with relatively long Na-S bond lengths, which significantly lowers the diffusion energy barrier (with an activation energy of 0.465 eV as shown in **Figure 2B**). According to the calculated probability distribution in **Figure 2C**,

around each moving row of Na-ions along the *c* axis, the four neighboring all-Na rows move in the opposite direction. This makes the nearest Na-ion rows always move away from each other, lowering the electrostatic energy due to the separation of the same charges.

In comparison, there are four types of cationic rows arranged alternately along each crystalline axis in the orthorhombic $Na_{2.7}W_{0.3}Sb_{0.7}S_4$ (**Figure 2A**). The first type contains only Na-ions (•••Na-Na-Na-Na•••). The second type contains alternate Na and Sb ions (•••Na-Sb-Na-Sb•••). These are also found in Na_3SbS_4. The third type contains alternate Na and Sb/W ions (•••Na-Sb-Na-W•••) and the fourth type contains alternate Na and W ions (•••Na-W-Na-W•••). Especially, the fourth type is only possible with heavy W-doping in $Na_{2.7}W_{0.3}Sb_{0.7}S_4$. Although only the first-type (•••Na-Na-Na-Na•••) rows are mobile, Na-ions from other row types can join the collective transport of the first-type rows by jumping into the Na-vacancies, as shown by the calculated probability distribution in **Figure 2C** (Left panel). As shown by the van Hove correlation function in **Figure 2D**, strong correlations between Na-ions up to the third nearest neighbor are found in both Na_3SbS_4 and $Na_{2.7}W_{0.3}Sb_{0.7}S_4$. The major difference of the two cases is the weakened correlation between the nearest neighboring Na-ions over time in $Na_{2.7}W_{0.3}Sb_{0.7}S_4$ (**Figure 2D**, left panel), which is due to the enhanced individual jumping into the nearest neighboring Na vacancies. Thus, the Na-vacancies and correlated Na-ion transport are the enablers for the observed three-dimensional fast-ion conduction in $Na_{2.7}W_{0.3}Sb_{0.7}S_4$.

The activation energy of the material is found to be closely related to the local interatomic interactions which are studied by the calculated radial distribution function (RDF) shown in **Figure 2E**. Fewer S interaction with each Na-ion in a structure and longer Na-S bond length will lead to weaker interaction strength and smaller migration barrier. The number of S ions interacting with each Na-ion and the averaged Na-S bond length are calculated by considering all the major peaks in the Na-S RDF of each case in **Figure 2E**. For example, in the cubic phase of Na_3SbS_4 which exhibits the exceptionally low activation energy, each Na atom is coordinated by 8 S atoms and each S is shared by 6 Na atoms. Therefore, each Na-ion is interacting with (8/6 =) 1.33 S in the cubic Na_3SbS_4 and the averaged Na-S bond length is 3.22 Å. It is found that each Na-ion in the orthorhombic $Na_{2.7}W_{0.3}Sb_{0.7}S_4$ is interacting with 1.40 S and the averaged Na-S bond length is 3.10 Å, which are close to the case of cubic Na_3SbS_4. In contrast, the averaged Na-S bond length

$<$ 3.0 Å of tetragonal Na_3SbS_4 is much shorter. The weak Na-S interaction found in the cubic Na_3SbS_4 is due to the high symmetry,[71] while that in the W-doped $Na_{2.7}W_{0.3}Sb_{0.7}S_4$ is enabled by W-S interactions. With an ionic radius very similar to that of Sb^{5+}, each W^{6+} in the doped system interacts more strongly with the four-coordinating S than that of Sb^{5+}, as shown by the much shorter W-S bond length than that of Sb-S in the calculated RDF (**Figure 2E**). Cationic rows (the third and fourth types mentioned above) containing W-ions can, therefore, hold the S ions much more closely, effectively lowering the Na-S interactions of the neighboring Na-ions and the activation energy of the material. Such effect is especially significant in the heavily W-doped system, where the fourth-type rows (•••Na-W-Na-W•••) with Sb entirely replaced by W are present in the structure (**Figure 2A**), leading to the very low activation energy of $Na_{2.7}W_{0.3}Sb_{0.7}S_4$.

Maintaining the advantages of heavy W-doping, the properties of $Na_{2.7}W_{0.3}Sb_{0.7}S_4$ can be further optimized by tuning the Na-vacancy content in the system using excess Na-ions. It seems that a system containing more vacancy sites would generate more possible energetically degenerate or nearly-degenerate states, enabling the Na sublattice to rearrange into and, therefore, increasing the ionic conductivity. According to this, a structure having 5 vacancies out of a total of 48 Na sites can generate $C_{48}^{43} = C_{48}^{5} = 1712304$ possible states for the Na-sublattice to occupy which is over 10^3 times more than the number of states ($C_{48}^{46} = C_{48}^{2} = 1128$) that can be generated by 2 vacancies out of 48 Na sites in a structure. Such great difference, according to the ion transport model,[74] should be reflected in the prefactor "A" of the Arrhenius ionic conductivity formalism $\sigma = A \times \exp(-E_a/RT)$. This term could readily overpower the Boltzmann factor $\exp(-E_a/RT)$ if the activation energies of the two structures are not very different, leading to much higher ionic conductivity in the structure containing more vacancies. However, other factors out of this overly simplified picture may come with the presence of vacancies and work adversely to the ionic conduction. For example, it has been found in $Na_{3-\delta}PS_{3.8}Cl_{0.2}$ systems that extra Na-vacancies reduce the size of diffusion channels and lower the ionic conductivity.[42] More vacancies can also lead to reduced ionic conductivity in grain boundaries due to the segregation of Na-vacancy,[75] which could be responsible for the large grain boundary resistance observed in the powder sample of $Na_{2.7}W_{0.3}Sb_{0.7}S_4$ (**Figure S3** of **SI**). On the other hand, it has been found that a small amount of excess Li- or Na-ions in lithium and sodium sulfide conductors, e.g., lithium argyrodites and Na_3PS_4, can promote ionic diffusion.[76,77]

Bearing these in mind, a new set of materials $Na_{3-\delta}W_xSb_{1-x}S_4$ (x = 0.1, 0.2 and 0.3; $0 < \delta < x$) are synthesized (Experimental Method in SI). Among the series, $Na_{2.895}W_{0.3}Sb_{0.7}S_4$ with heavy W-doping and excess Na-ions based on $Na_{2.7}W_{0.3}Sb_{0.7}S_4$ is found to have the best properties. Its structural model, as shown in **Figure 3A**, is obtained by first inserting three Na-ions back into the model of $Na_{2.7}W_{0.3}Sb_{0.7}S_4$ (**Figure 1A**) and then fully optimizing the structure using DFT. The ground-state structure of $Na_{2.895}W_{0.3}Sb_{0.7}S_4$ (a=14.1945, b=14.2463 and c=14.1948 Å; α=89.9964, β=89.9971 and γ=90.0023˚) can be viewed as a pseudo-cubic structure, with a high-symmetric Na-sublattice bearing high resemblance to that of the cubic phase of Na_3SbS_4, as shown by the calculated Na-Na RDFs in **Figure 2E**. The simulated XRD based on the structure model agrees well with the measured one and, therefore, a cubic phase is used to conduct the Rietveld refinement, as shown in **Figure 3B**. The refined lattice parameters (a=b=c=14.4184 Å; α=β=γ=90˚) are in good agreement with the calculated ones with relative differences less than 1.5%. As shown in **Figure 1C**, $Na_{2.895}W_{0.3}Sb_{0.7}S_4$ exhibits the same Raman signals at 370, 390, 410 and 470 cm^{-1} as in the case of $Na_{2.7}W_{0.3}Sb_{0.7}S_4$, suggesting the presence of SbS_4^{3-} and WS_4^{2-}. The measured electric conductivity of $Na_{2.895}W_{0.3}Sb_{0.7}S_4$ is more than one order of magnitude smaller than that of $Na_{2.7}W_{0.3}Sb_{0.7}S_4$, which is much desired. [78-79]

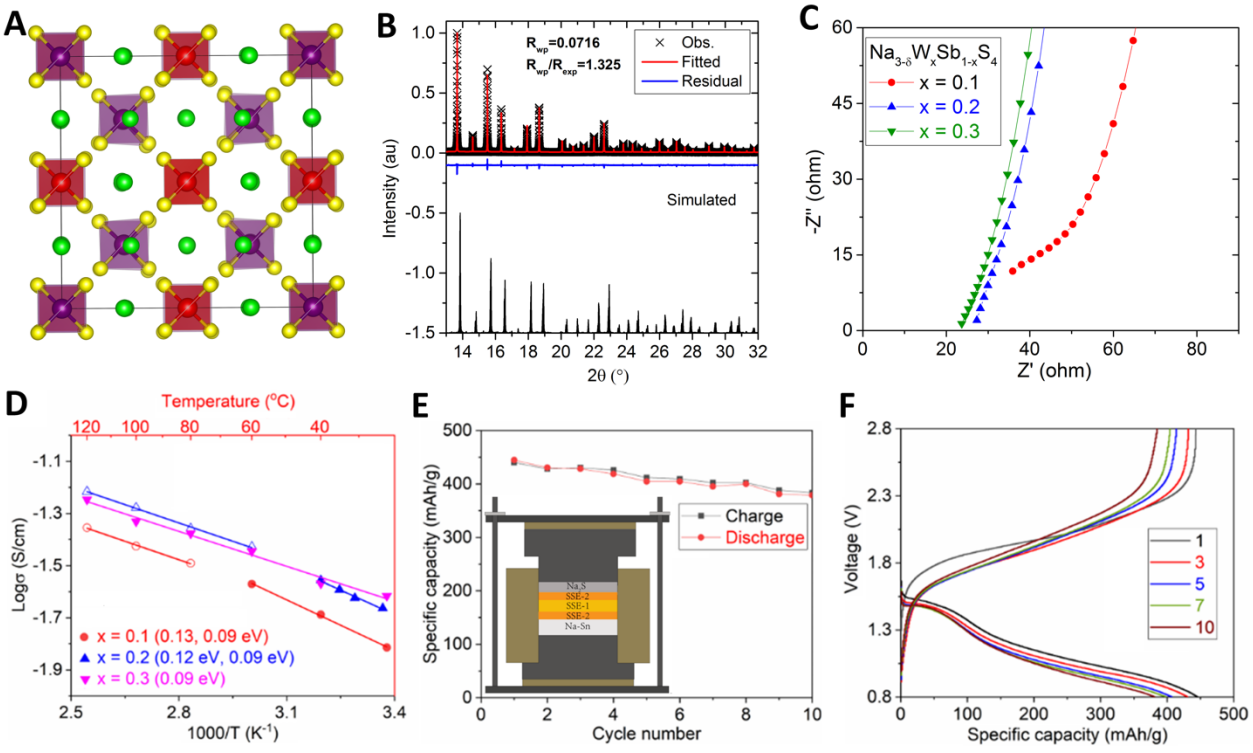

Fig. 3 Characterizations of $Na_{2.895}W_{0.3}Sb_{0.7}S_4$ and its implementation in an all-solid-state battery. (**A**) Theoretical obtained ground-state structure of $Na_{2.895}W_{0.3}Sb_{0.7}S_4$ featuring a pseudo-cubic structure (see Theoretical Method in SI), with SbS_4^{3-} units in purple, WS_4^{2-} units in red and Na in green. (**B**) Synchrotron XRD of $Na_{2.895}W_{0.3}Sb_{0.7}S_4$ and the Rietveld refinement based on a cubic model with fixed 3:7 W vs. Sb occupancy. The refined occupancy of Na is 0.965. (**C**) The measured AC impedances for the $Na_{3-\delta}W_xSb_{1-x}S_4$ (x = 0.1, 0.2 and 0.3; $0 < \delta < x$) series. (**D**) The measured ionic conductivities of the $Na_{3-\delta}W_xSb_{1-x}S_4$ (x = 0.1, 0.2 and 0.3; $0 < \delta < x$) series at different temperatures. (**E**) Cycling performance of the assembled all-solid-state battery using $Na_{2.895}W_{0.3}Sb_{0.7}S_4$ as the solid electrolyte. The inset shows the schematics of the battery cell, where two buffer layers of Na_3SbS_4 (SSE2) are put between $Na_{2.895}W_{0.3}Sb_{0.7}S_4$ (SSE1) and the electrodes. (**F**) The measured charge-discharge profiles of the Na_2S/SSE/Na_3Sn ASSB at different cycles.

As shown in **Figure 3C**, $Na_{2.895}W_{0.3}Sb_{0.7}S_4$ has the lowest bulk resistance of 23.7 Ω in the series. Similar to the case of $Na_{2.7}W_{0.3}Sb_{0.7}S_4$ and unlike the others in the series, $Na_{2.895}W_{0.3}Sb_{0.7}S_4$ shows no discontinuity in its measured ionic conductivities as shown in **Figure 3D**, suggesting that there is no phase transition. $Na_{2.895}W_{0.3}Sb_{0.7}S_4$ exhibits a record low activation energy of 0.09 eV and a RT ionic conductivity of 24.2 mS/cm. The calculated activation energy of 0.088 eV (**Fig. 2B**) is in excellent agreement with the experimental value. The calculated RT ionic conductivity of 56 mS/cm, which is much closer to the measured value than the case of $Na_{2.7}W_{0.3}Sb_{0.7}S_4$, suggests good sample quality of $Na_{2.895}W_{0.3}Sb_{0.7}S_4$. Indeed, measurements show that there is no significant grain boundary resistance in the sample (**Figure S3** of SI). This is consistent with the previous simple analysis. While more Na-vacancies can lead to higher ionic conductivities as shown by the calculated values of $Na_{2.7}W_{0.3}Sb_{0.7}S_4$ *vs*. $Na_{2.895}W_{0.3}Sb_{0.7}S_4$ in **Figure 2B**, it can also bring unfavorable factors as the large grain-boundary resistance in $Na_{2.7}W_{0.3}Sb_{0.7}S_4$, which greatly lowers the ionic conductivity in practice.

The record low activation energy of $Na_{2.895}W_{0.3}Sb_{0.7}S_4$ among all the known sulfide sodium solid electrolytes at RT (see **Table 1**) is due to the weak local Na-S interactions and enhanced Na-Na repulsion with excess Na-ions added in $Na_{2.7}W_{0.3}Sb_{0.7}S_4$. According to the RDF analysis in **Figure 2E**, $Na_{2.895}W_{0.3}Sb_{0.7}S_4$ is characterized by almost the same local Na-S interactions as in the cubic phase of Na_3SbS_4, having each Na-ion interacting with 1.33 S and an averaged Na-S bond

length of 3.17 Å. Such weak Na-S interaction in $Na_{2.895}W_{0.3}Sb_{0.7}S_4$ is enabled by two factors. One is the strong W-S interaction due to the heavy W-doping, pulling, especially, the S atoms close to the W-containing fourth-type cationic rows with all Sb substituted by W, as indicated by the W-S RDF in **Figure 2E**. The other is the high-symmetry Na-sublattice, which resembles that of the cubic phase of Na_3SbS_4,[71] as shown by the Na-Na RDFs in **Figure 2E**. In addition, the Na-Na correlation is enhanced due to the excess Na-ions in $Na_{2.895}W_{0.3}Sb_{0.7}S_4$ compared to that in $Na_{2.7}W_{0.3}Sb_{0.7}S_4$. This is shown by the Na-Na RDFs in **Figure 2E**, where the distances between a Na-ion and its first- and second-nearest neighbors (around 3.5 and 5.0 Å, respectively) become significantly shorter in $Na_{2.895}W_{0.3}Sb_{0.7}S_4$ compared to those of $Na_{2.7}W_{0.3}Sb_{0.7}S_4$ and cubic Na_3SbS_4. The enhanced Na-ion correlations in $Na_{2.895}W_{0.3}Sb_{0.7}S_4$ increases the Na-Na repulsion and, therefore, further lowers the energy barrier and the activation energy for the Na-ion diffusion.

Table 1. Comparison of key properties of the known sulfide sodium solid electrolytes, showing that the heavily W-doped systems in this study exhibit the highest RT ionic conductivities and the lowest activation energies.

Solid state electrolyte	**SSE preparation**	**Crystal system**	**σ at RT (mS/cm)**	**E_a (eV)**	**Ref.**
$Na_{2.7}W_{0.3}Sb_{0.7}S_4$	Cold pressed with 350 MPa	Orthorhombic	14.5	0.12	**This work**
$Na_{2.895}W_{0.3}Sb_{0.7}S_4$	Cold pressed with 350 MPa	Cubic	24.2	0.09	**This work**
Na_3PS_4	Cold pressed and heated at 270 °C	Cubic	0.2	0.28	[52]
$Na_{2.9375}PS_{3.9375}Cl_{0.0625}$	Spark plasma sintering, 100 MPa, 300 °C for 5 min	Tetragonal	1.14	0.25	[54]
$Na_{3-\delta}PS_{3.8}Cl_{0.2}$	Cold pressed, heated at 420 °C and then natural cooling to RT	Tetragonal	2	0.19	[42]
$Na_{2.73}Ca_{0.135}PS_4$	Cold pressed at 370 MPa	Cubic	1	0.49	[39]
Na_3PSe_4	Cold pressed at 400 MPa	Cubic	1.16	0.21	[41]
$Na_3P_{0.62}As_{0.38}S_4$	Cold pressed at 400 MPa	Tetragonal	1.46	0.256	[44]
Na_3SbS_4	Cold pressed with 480 MPa	Tetragonal	0.5	0.224	[53]

Na_3SbS_4	Cold pressed	Tetragonal	3	0.25	[45]
$Na_{2.88}W_{0.12}Sb_{0.88}S_4$	Cold pressed with 1080 MPa and sintered at 275 ℃	Cubic	32	0.21	[37]
$Na_{2.9}W_{0.1}Sb_{0.9}S_4$	Cold pressed with 380 MPa, heated at 550 ℃ and then quenched to RT	Cubic	41	0.18	[36]
$Na_{10}SnP_2S_{12}$	Cold pressed and sintered at 700 ℃ for 12 h	Tetragonal	0.4	0.356	[80]
$Na_{11}Sn_2PS_{12}$	Cold pressed and sintered at 700 ℃ for 2 h, slow cooling for 99 h from 700 to 250 ℃	Tetragonal	1.4	0.25	[81]
$Na_{11}Sn_2PS_{12}$	Cold pressed and sintered at 600 ℃	Tetragonal	3.7	0.383	[82]

Owing to the record-low activation energy, $Na_{2.895}W_{0.3}Sb_{0.7}S_4$ remains a good ionic conductor, well below the freezing temperature. At −15 ℃, its measured bulk ionic conductivity is 23 mS/cm and, even with increased grain-boundary resistance at such a low temperature, its total ionic conductivity is still a good operative value of 5.5 mS/cm (**Figure S4** of SI). A stable all-solid-state battery (ASSB), as shown schematically in **Figure 3E** (inset), is successfully assembled using $Na_{2.895}W_{0.3}Sb_{0.7}S_4$ as solid electrolyte, Na_3Sn as anode and Na_2S as cathode. With direct contact to the electrodes, $Na_{2.895}W_{0.3}Sb_{0.7}S_4$ will turn into a mixed conductor after being partially reduced to $Na_{3.3}W_{0.3}Sb_{0.7}S_4$ (**Figure S5** of SI). This makes the electrode-electrolyte interfaces (EEI) become unstable and the battery capacity decays fast (**Figure S6** of SI). It is found that using two buffer layers of Na_3SbS_4 to sandwich the solid electrolyte can greatly improve the EEI stability and the resulting ASSB shows good cycle performance with a high capacity maintained around 400 mAh/g, as shown in **Figure 3E** and **3F**. Application of artificially stable EEI layer (such as the case here of $Na_{2.895}W_{0.3}Sb_{0.7}S_4$) is quite common in high performance ASSBs. For example, sodiated alucone on the surface of Na metal anode may help to stabilize the EEI.[43]

Conclusion

Two sodium solid electrolytes, $Na_{2.895}W_{0.3}Sb_{0.7}S_4$ and $Na_{2.7}W_{0.3}Sb_{0.7}S_4$, have been fabricated with activation energies of 0.09 and 0.12 eV, which are among the lowest values reported in the literature. The solid electrolytes also exhibit very high RT ionic conductivities of 24.2 and 14.5 mS/cm, respectively. Especially, $Na_{2.895}W_{0.3}Sb_{0.7}S_4$ exhibits very low grain-boundary resistance and electric conductivity, and can support a stable all-solid-state battery operating at high capacity. It is found that the superior properties of these solid electrolytes, especially the record low activation energy, originate from multiple mechanistic principles that support fast-ion diffusion. The uniquely heavy W-doping (with 30% W *vs*. Sb in the system) creates special structural configurations (e.g., the •••Na-W-Na-W••• rows) that lower the local Na-S interactions by pulling the S away from Na-ions through the strong W-S interaction. Introducing additional Na-ions in the stoichiometric $Na_{2.7}W_{0.3}Sb_{0.7}S_4$ creates slight Na-excess in the non-stoichiometric $Na_{2.895}W_{0.3}Sb_{0.7}S_4$, which in turn enhances the Na-Na correlations. This further lowers the Na-ion migration barrier, and simultaneously optimizes the vacancy content of the system to avoid large grain-boundary resistance.

Acknowledgements

This research was supported by the U.S. Department of Energy, Office of Basic Energy Sciences, Division of Materials Sciences and Engineering under Award No.DE-FG02-96ER45579 and U.S. Department of Energy under Award No. DE-EE0008865. This research used resources of the National Energy Research Scientific Computing Center; a DOE Office of Science User Facility supported by the Office of Science of the U.S. Department of Energy under Contract No. DE-AC02-05CH11231.

References

[1] Y. Qi, C. Ban, S. J. Harris, *Joule* **2020**, *4*, 2599.

[2] Y. Zhao, K. Zheng, X. Sun, *Joule* **2018**, *2*, 2583.

[3] D. H. S. Tan, A. Banerjee, Z. Chen, Y. S. Meng, *Nat. Nanotechnol.* **2020**, *15*, 170.

[4] S. Lou, F. Zhang, C. Fu, M. Chen, Y. Ma, G. Yin, J. Wang, *Adv. Mater.* **2021**, *33*, 2000721.

[5] L. Xu, S. Tang, Y. Cheng, K. Wang, J. Liang, C. Liu, Y.-C. Cao, F. Wei, L. Mai, *Joule* **2018**, *2*, 1991.

[6] K. J. Huang, G. Ceder, E. A. Olivetti, *Joule* **2021**, *5*, 564.

[7] X. Judez, G. G. Eshetu, C. Li, L. M. Rodriguez-Martinez, H. Zhang, M. Armand, *Joule* **2018**, *2*, 2208.

[8] F. Duffner, N. Kronemeyer, J. Tübke, J. Leker, M. Winter, R. Schmuch, *Nat Energy* **2021**, *6*, 123.

[9] M. Balaish, J. C. Gonzalez-Rosillo, K. J. Kim, Y. Zhu, Z. D. Hood, J. L. M. Rupp, *Nat Energy* **2021**, *6*, 227.

[10] N. Zhao, W. Khokhar, Z. Bi, C. Shi, X. Guo, L.-Z. Fan, C.-W. Nan, *Joule* **2019**, *3*, 1190.

[11] A. M. Abakumov, S. S. Fedotov, E. V. Antipov, J.-M. Tarascon, *Nat Commun* **2020**, *11*, 4976.

[12] Y. Shen, Y. Zhang, S. Han, J. Wang, Z. Peng, L. Chen, *Joule* **2018**, *2*, 1674.

[13] J. Nanda, C. Wang, P. Liu, *MRS Bull.* **2018**, *43*, 740.

[14] P. Albertus, V. Anandan, C. Ban, N. Balsara, I. Belharouak, J. Buettner-Garrett, Z. Chen, C. Daniel, M. Doeff, N. J. Dudney, B. Dunn, S. J. Harris, S. Herle, E. Herbert, S. Kalnaus, J. A. Libera, D. Lu, S. Martin, B. D. McCloskey, M. T. McDowell, Y. S. Meng, J. Nanda, J.

Sakamoto, E. C. Self, S. Tepavcevic, E. Wachsman, C. Wang, A. S. Westover, J. Xiao, T. Yersak, *ACS Energy Lett.* **2021**, 1399.

[15] T. Famprikis, P. Canepa, J. A. Dawson, M. S. Islam, C. Masquelier, *Nat. Mater.* **2019**, *18*, 1278.

[16] T. Krauskopf, F. H. Richter, W. G. Zeier, J. Janek, *Chem. Rev.* **2020**, acs.chemrev.0c00431.

[17] Y. Gao, A. M. Nolan, P. Du, Y. Wu, C. Yang, Q. Chen, Y. Mo, S.-H. Bo, *Chem. Rev.* **2020**, *120*, 5954.

[18] A. Banerjee, X. Wang, C. Fang, E. A. Wu, Y. S. Meng, *Chem. Rev.* **2020**, *120*, 6878.

[19] G. G. Eshetu, G. A. Elia, M. Armand, M. Forsyth, S. Komaba, T. Rojo, S. Passerini, *Adv. Energy Mater.* **2020**, *10*, 2000093.

[20] Y. Kato, S. Hori, T. Saito, K. Suzuki, M. Hirayama, A. Mitsui, M. Yonemura, H. Iba, R. Kanno, *Nature Energy* **2016**, *1*, 16030.

[21] Y.-G. Lee, S. Fujiki, C. Jung, N. Suzuki, N. Yashiro, R. Omoda, D.-S. Ko, T. Shiratsuchi, T. Sugimoto, S. Ryu, J. H. Ku, T. Watanabe, Y. Park, Y. Aihara, D. Im, I. T. Han, *Nat Energy* **2020**, *5*, 299.

[22] M. J. Wang, R. Choudhury, J. Sakamoto, *Joule* **2019**, *3*, 2165.

[23] P. Panigrahi, Y. Pal, T. Hussain, R. Ahuja, *Applied Surface Science* **2021**, *558*, 149850.

[24] A. Patra, J. Davis, S. Pidaparthy, M. H. Karigerasi, B. Zahiri, A. A. Kulkarni, M. A. Caple, D. P. Shoemaker, J. M. Zuo, P. V. Braun, *Proceedings of the National Academy of Sciences* **2021**, *118*, DOI 10.1073/pnas.2025044118.

[25] C. Bao, B. Wang, P. Liu, H. Wu, Y. Zhou, D. Wang, H. Liu, S. Dou, *Advanced Functional Materials* **2020**, *30*, 2004891.

[26] G. Cui, *Matter* **2020**, *2*, 805.

[27] K. Kalaga, M.-T. F. Rodrigues, H. Gullapalli, G. Babu, L. M. R. Arava, P. M. Ajayan, *ACS Appl. Mater. Interfaces* **2015**, *7*, 25777.

[28] P. Jaumaux, J. Wu, D. Shanmukaraj, Y. Wang, D. Zhou, B. Sun, F. Kang, B. Li, M. Armand, G. Wang, *Advanced Functional Materials* **2021**, *31*, 2008644.

[29] X. Guo, J. Bae, Y. Ding, X. Zhang, G. Yu, *Advanced Functional Materials* **2021**, *31*, 2010863.

[30] X. Gao, X. Zheng, J. Wang, Z. Zhang, X. Xiao, J. Wan, Y. Ye, L.-Y. Chou, H. K. Lee, J. Wang, R. A. Vilá, Y. Yang, P. Zhang, L.-W. Wang, Y. Cui, *Nano Lett.* **2020**, *20*, 5496.

[31] C. Wang, K. Fu, S. P. Kammampata, D. W. McOwen, A. J. Samson, L. Zhang, G. T. Hitz, A. M. Nolan, E. D. Wachsman, Y. Mo, V. Thangadurai, L. Hu, *Chem. Rev.* **2020**, *120*, 4257.

[32] Y.-L. Ding, P. Kopold, K. Hahn, P. A. van Aken, J. Maier, Y. Yu, *Advanced Functional Materials* **2016**, *26*, 1112.

[33] Y. Pang, J. Pan, J. Yang, S. Zheng, C. Wang, *Electrochemical Energy Reviews* **2021**, *4*, 169.

[34] J. Bae, X. Zhang, X. Guo, G. Yu, *Nano Lett.* **2021**, *21*, 1184.

[35] H. Yuan, H. Li, T. Zhang, G. Li, T. He, F. Du, S. Feng, *J. Mater. Chem. A* **2018**, *6*, 8413.

[36] T. Fuchs, S. P. Culver, P. Till, W. G. Zeier, *ACS Energy Lett.* **2020**, *5*, 146.

[37] A. Hayashi, N. Masuzawa, S. Yubuchi, F. Tsuji, C. Hotehama, A. Sakuda, M. Tatsumisago, *Nat Commun* **2019**, *10*, 5266.

[38] E. A. Wu, C. S. Kompella, Z. Zhu, J. Z. Lee, S. C. Lee, I.-H. Chu, H. Nguyen, S. P. Ong, A. Banerjee, Y. S. Meng, *ACS Applied Materials & Interfaces* **2018**, *10*, 10076.

[39] C. K. Moon, H.-J. Lee, K. H. Park, H. Kwak, J. W. Heo, K. Choi, H. Yang, M.-S. Kim, S.-T. Hong, J. H. Lee, Y. S. Jung, *ACS Energy Lett.* **2018**, *3*, 2504.

[40] T. Famprikis, J. A. Dawson, F. Fauth, O. Clemens, E. Suard, B. Fleutot, M. Courty, J.-N. Chotard, M. S. Islam, C. Masquelier, *ACS Materials Lett.* **2019**, *1*, 641.

[41] L. Zhang, K. Yang, J. Mi, L. Lu, L. Zhao, L. Wang, Y. Li, H. Zeng, *Adv. Energy Mater.* **2015**, *5*, 1501294.

[42] X. Feng, P.-H. Chien, Z. Zhu, I.-H. Chu, P. Wang, M. Immediato-Scuotto, H. Arabzadeh, S. P. Ong, Y.-Y. Hu, *Adv. Funct. Mater.* **2019**, *29*, 1807951.

[43] S. Zhang, Y. Zhao, F. Zhao, L. Zhang, C. Wang, X. Li, J. Liang, W. Li, Q. Sun, C. Yu, J. Luo, K. Doyle-Davis, R. Li, T. Sham, X. Sun, *Adv. Funct. Mater.* **2020**, *30*, 2001118.

[44] Z. Yu, S.-L. Shang, J.-H. Seo, D. Wang, X. Luo, Q. Huang, S. Chen, J. Lu, X. Li, Z.-K. Liu, D. Wang, *Advanced Materials* **2017**, *29*, 1605561.

[45] L. Zhang, D. Zhang, K. Yang, X. Yan, L. Wang, J. Mi, B. Xu, Y. Li, *Advanced Science* **2016**, *3*, 1600089.

[46] H. Wang, Y. Chen, Z. D. Hood, G. Sahu, A. S. Pandian, J. K. Keum, K. An, C. Liang, *Angew. Chem.* **2016**, *128*, 8693.

[47] A. Banerjee, K. H. Park, J. W. Heo, Y. J. Nam, C. K. Moon, S. M. Oh, S.-T. Hong, Y. S. Jung, *Angew. Chem. Int. Ed.* **2016**, *55*, 9634.

[48] Z. Zhu, I.-H. Chu, Z. Deng, S. P. Ong, *Chem. Mater.* **2015**, *27*, 8318.

[49] T. Krauskopf, S. P. Culver, W. G. Zeier, *Inorg. Chem.* **2018**, *57*, 4739.

[50] S. Yubuchi, A. Ito, N. Masuzawa, A. Sakuda, A. Hayashi, M. Tatsumisago, *J. Mater. Chem. A* **2020**, *8*, 1947.

[51] S. Takeuchi, K. Suzuki, M. Hirayama, R. Kanno, *Journal of Solid State Chemistry* **2018**, *265*, 353.

[52] A. Hayashi, K. Noi, A. Sakuda, M. Tatsumisago, *Nat Commun* **2012**, *3*, 856.

[53] Q. Zhang, C. Zhang, Z. D. Hood, M. Chi, C. Liang, N. H. Jalarvo, M. Yu, H. Wang, *Chem. Mater.* **2020**, *32*, 2264.

[54] I.-H. Chu, C. S. Kompella, H. Nguyen, Z. Zhu, S. Hy, Z. Deng, Y. S. Meng, S. P. Ong, *Scientific Reports* **2016**, *6*, DOI 10.1038/srep33733.

[55] N. Tanibata, K. Noi, A. Hayashi, M. Tatsumisago, *RSC Adv.* **2014**, *4*, 17120.

[56] H. Nguyen, A. Banerjee, X. Wang, D. Tan, E. A. Wu, J.-M. Doux, R. Stephens, G. Verbist, Y. S. Meng, *Journal of Power Sources* **2019**, *435*, 126623.

[57] A. Hayashi, K. Noi, N. Tanibata, M. Nagao, M. Tatsumisago, *Journal of Power Sources* **2014**, *258*, 420.

[58] N. Wang, K. Yang, L. Zhang, X. Yan, L. Wang, B. Xu, *J Mater Sci* **2018**, *53*, 1987.

[59] C. Yu, S. Ganapathy, N. J. J. de Klerk, E. R. H. van Eck, M. Wagemaker, *J. Mater. Chem. A* **2016**, *4*, 15095.

[60] S. Nishimura, N. Tanibata, A. Hayashi, M. Tatsumisago, A. Yamada, *J. Mater. Chem. A* **2017**, *5*, 25025.

[61] S.-H. Bo, Y. Wang, G. Ceder, *Journal of Materials Chemistry A* **2016**, *4*, 9044.

[62] Z. Zhang, H. Cao, M. Yang, X. Yan, C. Yu, D. Liu, L. Zhang, *Journal of Energy Chemistry* **2020**, *48*, 250.

[63] X. Xu, Y. Li, J. Cheng, G. Hou, X. Nie, Q. Ai, L. Dai, J. Feng, L. Ci, *Journal of Energy Chemistry* **2020**, *41*, 73.

[64] Q. Zhang, C. Zhang, Z. D. Hood, M. Chi, C. Liang, N. H. Jalarvo, M. Yu, H. Wang, *Chem. Mater.* **2020**, *32*, 2264.

[65] N. J. J. de Klerk, M. Wagemaker, *Chemistry of Materials* **2016**, *28*, 3122.

[66] N. Tanibata, M. Deguchi, A. Hayashi, M. Tatsumisago, *Chemistry of Materials* **2017**, *29*, 5232.

[67] **N.d.**

[68] J. A. Dawson, P. Canepa, T. Famprikis, C. Masquelier, M. S. Islam, *J. Am. Chem. Soc.* **2018**, *140*, 362.

[69] D. Zhang, X. Cao, D. Xu, N. Wang, C. Yu, W. Hu, X. Yan, J. Mi, B. Wen, L. Wang, L. Zhang, *Electrochimica Acta* **2018**, *259*, 100.

[70] B. Kozinsky, in *Handbook of Materials Modeling: Applications: Current and Emerging Materials* (Eds.: W. Andreoni, S. Yip), Springer International Publishing, Cham, **2018**, pp. 1–20.

[71] Q. Zhang, C. Zhang, Z. D. Hood, M. Chi, C. Liang, N. H. Jalarvo, M. Yu, H. Wang, *Chem. Mater.* **2020**, *32*, 2264.

[72] Z. Deng, Z. Zhu, I.-H. Chu, S. P. Ong, *Chemistry of Materials* **2017**, *29*, 281.

[73] J. A. Dawson, P. Canepa, T. Famprikis, C. Masquelier, M. S. Islam, *J. Am. Chem. Soc.* **2018**, 7.

[74] M. J. Rice, W. L. Roth, *Journal of Solid State Chemistry* **1972**, *4*, 294.

[75] K. Shen, R. He, Y. Wang, C. Zhao, H. Chen, *J. Phys. Chem. C* **2020**, *124*, 26241.

[76] Z. Zhu, I.-H. Chu, Z. Deng, S. P. Ong, *Chem. Mater.* **2015**, *27*, 8318.

[77] Z. Deng, Z. Zhu, I.-H. Chu, S. P. Ong, *Chem. Mater.* **2017**, *29*, 281.

[78] F. Han, A. S. Westover, J. Yue, X. Fan, F. Wang, M. Chi, D. N. Leonard, N. J. Dudney, H. Wang, C. Wang, *Nat Energy* **2019**, *4*, 187.

[79] M. Philipp, B. Gadermaier, P. Posch, I. Hanzu, S. Ganschow, M. Meven, D. Rettenwander, G. J. Redhammer, H. M. R. Wilkening, *Adv. Mater. Interfaces* **2020**, *7*, 2000450.

[80] W. D. Richards, T. Tsujimura, L. J. Miara, Y. Wang, J. C. Kim, S. P. Ong, I. Uechi, N. Suzuki, G. Ceder, *Nature Communications* **2016**, *7*, DOI 10.1038/ncomms11009.

[81] Z. Zhang, E. Ramos, F. Lalère, A. Assoud, K. Kaup, P. Hartman, L. F. Nazar, *Energy & Environmental Science* **2018**, *11*, 87.

[82] M. Duchardt, U. Ruschewitz, S. Adams, S. Dehnen, B. Roling, *Angewandte Chemie International Edition* **2018**, *57*, 1351.